





Cite this: DOI: 10.1039/d5ay01060h

Dual-output entropy-driven catalytic amplification coupled with G-quadruplex dimers for ultrasensitive label-free detection of miRNA-21

Chuan Long,^a Yao Yao,^a Ziyi Gao,^a Qi Liu ^{*a} and Xiaoqing Chen ^{ab}

The connection between aberrant expression of microRNAs (miRNAs) and tumorigenesis positions miRNAs as promising targets for early cancer detection. However, the low abundance of miRNAs in biological fluids, such as blood, presents significant challenges that necessitate the development of highly sensitive detection platforms. In this study, we present a label-free fluorescent biosensor that utilizes a dual-output entropy-driven catalytic (EDC) amplification system in conjunction with G-quadruplex (G4) dimer-mediated signal enhancement for the ultrasensitive detection of miRNA-21. The synergistic effect of the EDC-based signal amplification and the high fluorescence quantum yield of G4 dimers resulted in a biosensor with outstanding sensitivity. The platform demonstrated a linear response over a concentration range from 0.1 pM to 100 pM ($R^2 = 0.998$), with a limit of detection (LOD) calculated at 82 fM ($S/N = 3$). Specificity assays verified the biosensor's ability to accurately distinguish miRNA-21 from sequences with single, two, or three nucleotide mismatches, as well as from homologous miRNAs, underscoring its robust sequence selectivity. Furthermore, the biosensor's performance was assessed in human serum matrices, achieving recoveries between 96.2% and 104.8% and relative standard deviations below 2.4%. These results validate the biosensor's potential for clinical diagnostics, showcasing its efficacy and reliability in a complex biological environment.

Received 25th June 2025
Accepted 4th August 2025DOI: 10.1039/d5ay01060h
rsc.li/methods

Introduction

Cancer, a life-threatening condition, has garnered extensive global attention due to its significant impact on public health.^{1,2} Early diagnosis of cancer is critical for timely intervention and effective therapeutic strategies. As an important class of biomarkers, microRNAs (miRNAs),^{3–6} play essential regulatory roles in various biological processes such as cell proliferation^{7,8} and apoptosis.^{9,10} During carcinogenesis, specific miRNAs often exhibit marked upregulation or downregulation,^{3,6} facilitating non-invasive diagnosis through the detection of changes in miRNA concentrations in body fluids. This approach holds considerable promise for early cancer treatment and prognosis.^{3,4} However, challenges such as low miRNA abundance, high sequence homology, and interference from complex biological matrices pose significant hurdles to reliable detection, highlighting the urgent need for the development of sensitive and specific biosensors.

Numerous methods have been explored for the detection of miRNA, including microarray analysis^{11,12} and quantitative reverse transcription polymerase chain reaction (qRT-PCR).^{13,14} Although qRT-PCR is regarded as the gold standard, it has some

limitations such as cumbersome procedures, stringent temperature control requirements, and insufficient sensitivity. Therefore, it is imperative to employ signal amplification strategies to achieve both accurate and sensitive detection of target miRNAs.

Conventional signal amplification strategies for nucleic acid assay can be categorized into enzyme-assisted^{15–17} and enzyme-free approaches.^{18–22} Enzyme-free methods, which avoid the constraints of enzymatic processes and offer cost-effectiveness, have gained popularity for miRNA detection. Notable techniques include catalytic hairpin assembly (CHA),^{23–27} hybridization chain reaction (HCR),^{28–30} and entropy-driven catalytic (EDC).^{31–33} While CHA and HCR involve intricate hairpin structure designs, EDC employs single-stranded DNA components, providing simplicity and efficient signal amplification. However, traditional EDC systems underutilize output strands, leading to resource inefficiency. Enhancing the utilization of EDC output strands could enhance atomic economy and amplification efficiency, thereby optimizing the EDC platform. Currently, various signal output modalities are linked with EDC amplification cycles, such as fluorescence,^{32,33} Raman,^{34–36} and electrochemical signals.^{37–39} Among these, fluorescent biosensors^{19,25} are particularly favored for their stable signals, making them suitable for quantitative analysis. Fluorescent substances, including fluorophores,³³ quantum dots,^{31,40} and G-quadruplex (G4) structures, have been effectively combined with thioflavin

^aCollege of Chemistry and Chemical Engineering, Central South University, Changsha 410083, China. E-mail: iliuqi@csu.edu.cn; Tel: +86-731-88830833

^bXiangjiang Laboratory, Changsha 410205, China. E-mail: xqchen@csu.edu.cn

T (ThT) to produce significant fluorescence while maintaining cost-effectiveness and versatility.⁴¹ G4 structures,⁴² which are guanine-rich DNA sequences capable of folding into specific tertiary conformations in the presence of metal ions (*e.g.*, Na⁺ and K⁺), exhibit strong and stable fluorescence upon binding with ThT.^{43,44} However, using G4 and ThT alone for fluorescence detection has limitations that hinder their broader application. For example, while 22AG-derived G4 exhibits the highest ThT fluorescence enhancement, it is unsuitable as a fluorescence indicator for bioassays.⁴⁵ Recent investigations have shown that G4 dimers produce significantly enhanced fluorescence compared to G4 monomers under identical conditions, making them particularly advantageous for biosensor construction.⁴⁶

Motivated by these findings, we developed a novel fluorescent biosensor that integrates EDC dual-signal output with G4 dimers for the ultrasensitive detection of miRNA, specifically miRNA-21, as a proof of concept. The biosensor operates *via* a comprehensive DNA recycling circuit (Scheme 1) composed of an entropy-driven amplification reaction and an encapsulated G4 dimer (named DP). The whole mechanism diagram mainly consists of two parts, I and II. I consist of the 1 to 4 parts of the diagram, which represents the double-output EDC reaction. The EDC reaction is triggered when miRNA-21 and the fuel strand H4 are present. Through the successive strand displacement reactions, the 1 to 4 reaction process is driven to produce two DNA single strands H2 and H3, while miRNA-21 is continuously involved in the next EDC reaction process. Then, II consists of 5 and 6 parts of the scheme; 5 represents the process of the G4 dimer being encapsulated by BP to produce a DP-BP complex, which restricts the fluorescence signal generating ability of the G4 dimer. 6 represents that after the interaction of DP-BP with H2 and H3, the G4 dimer is released. In the presence of Na⁺, the released DP folds into a specific topology and binds to ThT, generating the desired fluorescent signal. This strategy offers two principal advantages: (1) improved resource utilization by fully exploiting EDC output strands and (2) enhanced sensitivity for miRNA detection through G4 dimer-mediated signal amplification. The proposed platform thus

presents a simple, cost-effective, and efficient approach for miRNA analysis, with broad applicability in clinical diagnostics.

Experimental

Reagents and apparatus

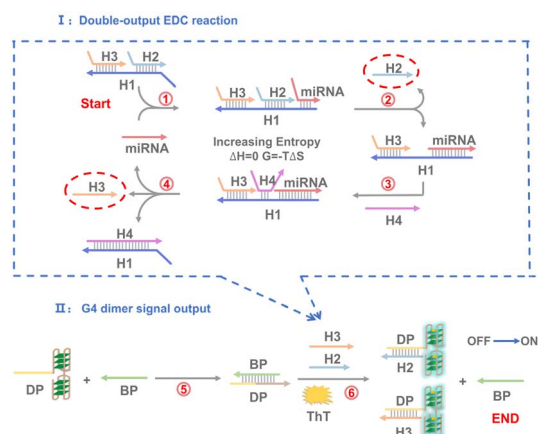
The detailed description of the reagents and instruments used in the experimental process can be found in the SI. The nucleic acid sequences employed are listed in Table S1.

Agarose gel electrophoresis (AGE) and polyacrylamide gel electrophoresis (PAGE)

To assess the functionality of the designed double-output EDC reaction, we performed AGE using a 3% gel. The gel was prepared by dissolving 900 mg of agarose powder in 30 mL of 1× TBE buffer, followed by heating and cooling. For each lane, 5 µL of the prepared reaction mixture was combined with 1 µL of loading buffer, yielding 6 µL of this mixture for electrophoresis. The agarose gel was run in 1× TBE buffer at a constant voltage of 120 V on ice for 45 min and then subsequently analysed using a gel imaging system under 365 nm UV irradiation. For improved resolution, we used 10% PAGE to verify the entire reaction process. To prepare 10% PAGE, 1.5 mL of a 40% acryl/bis solution (19:1 ratio) was mixed with 4.5 mL of 1× TBE buffer and 60 µL of APS. After thorough mixing, 5 µL of TEMED was added, and the solution was quickly poured into a casting mold. Polymerization was allowed to proceed for 10 min. Sample preparation, electrophoresis, and imaging were carried out as described for the agarose gel. The initial concentration of the DNA chains was 1 µM.

Fluorescence test analysis

All DNA strands were dissolved in TE buffer (10 mM Tris-HCl, 1 mM EDTA, pH = 7.6) according to the procedure in the instruction manual. The strands involved were heated at 95 °C for 10 min and then cooled naturally to room temperature, after which they were stored at 4 °C for further use. For the experiments, 0.5 µM H1, H2, and H3 were mixed in a 200 µL Eppendorf tube in volumes of 10 µL each, heated at 95 °C for 10 min, and then naturally allowed to cool to form the ternary complex H1-H2-H3. Similarly, the binary complex DP-BP was formed by mixing 10 µL of 1 µM DP and 10 µL of 1 µM BP using the same heating and cooling procedure. The ternary complex and binary complex solutions were then combined and supplemented with 10 µL each of 0.5 µM H4, 100 µM ThT, and 100 nM miRNA-21. Finally, 20 µL of reaction buffer solution (pH = 7.6, 50 mM Tris-HCl, 500 mM NaCl) was added to reach a final volume of 100 µL. The mixture was incubated at 35 °C for 4 h, after which fluorescence was measured using a fluorometer F-7000. The instrument was set at a voltage of 600 V, with excitation and emission slits both at 10 nm, at an excitation wavelength of 425 nm, and at an emission spectral range of 450 to 570 nm. In the control group, 10 µL of 100 nM miRNA-21 was substituted with 10 µL of the reaction buffer. The change in fluorescence intensity (ΔF) was defined as $\Delta F = F - F_0$, where F represents the fluorescence response in the presence of miRNA-21 and F_0



Scheme 1 Schematic diagram of dual-output EDC amplification coupled with G-4.

represents the response in its absence. Other experimental groups only need to change the corresponding DNA strands, while keeping everything else consistent.

Detection performance analysis

Under optimized experimental conditions, 10 μL of miRNA-21 solution with varying concentrations (0.0001 nM, 0.0005 nM, 0.001 nM, 0.005 nM, 0.01 nM, 0.05 nM, and 0.1 nM) were individually added to the reaction solution according to the aforementioned fluorescence testing protocol. The fluorescence values observed at these varying concentrations were then adjusted by subtracting the control group fluorescence values measured without miRNA-21 to yield the final fluorescence difference ΔF .

Selective testing and serum sample testing

To assess the selectivity of the developed method, three mutant miRNAs, including single-base mutation (named M1), double-base mutation (named M2), and triple-base mutation (named M3), and two homologous miRNAs (let-7a and let-7b) were selected as replacements for miRNA-21. The experimental protocol involved substituting miRNA-21 with 10 μL of 100 nM of the respective mutant or homologous miRNAs for fluorescence detection. Additionally, four concentrations of miRNA-21 were spiked into 1% serum samples to evaluate recovery through fluorescence measurements.

Results and discussion

Feasibility analysis of the biosensor

The two-dimensional structure of the experimental chain was simulated using the NUPACK simulation software and is presented in Fig. S1. To evaluate the feasibility of the proposed sensing system, we characterized the EDC dual signal output coupled with G4 dimer signal amplification *via* AGE (Fig. 1B)

and Fig. 1A shows the mechanism diagram of Fig. 1B. Lanes 1–5 correspond to the components miRNA-21, H1, H2, H3, and H4, respectively. Lane 6, representing a mixture of H1, H2, and H3, shows a single prominent band, confirming the successful formation of the ternary complex product H1–H2–H3. However, when H1–H2–H3 was combined with H4, lane 7 displays a weaker band indicative of the H1–H4 complex product, suggesting some background interference in the reaction. Lane 8 reveals a prominent band for the H1–H3–miRNA-21 complex upon the addition of target miRNA-21, with nearly complete disappearance of the ternary complex, confirming that H2 had been effectively replaced by the target miRNA. Subsequently, upon mixing miRNA-21, fuel chain H4, and H1–H2–H3, lane 9 reveals an intensified band for H1–H4, while the bands corresponding to H1–miRNA-21–H3 and H1–H2–H3 diminished, indicating the successful completion of the entire EDC reaction.

Besides, we employed 10% PAGE to resolve the bands better. Fig. 1C shows the diagram of the mechanism illustrated in Fig. 1D. As shown in Fig. 1D, lanes 1 and 2 represent the individual bands of DP and BP, respectively. Lane 3 shows the DP–BP complex. The addition of H2 and H3 (lane 4) produced a band migrating higher than the DP–BP complex, along with the presence of the BP band, suggesting that H2 and H3 displace BP by reacting with DP–BP. However, lane 5 shows no new band when H4 was mixed with DP–BP, indicating that H4 does not interact with DP–BP. In lane 6, when the ternary complex H1–H2–H3 was mixed with DP–BP, no H2–DP or H3–DP band was observed, indicating a lack of reaction. Following the introduction of miRNA-21, lane 7 exhibits a H2–DP band, confirming the previous observations that H2, displaced by miRNA-21, could react with DP–BP. Furthermore, lanes 8 and 9 show H1–H4, H2–DP, and H3–DP bands, along with a darker BP band, confirming the interaction of the EDC reaction product with DP–BP.

These findings confirmed the effective design of the EDC dual-output reaction in synergy with the G4 dimer. To further validate this system for miRNA-21 detection, we tested the signal amplification capabilities of single-output and dual-output EDC reactions. H1–*n*H2–H3 represents the construct lacking the H2 signal output, H1–H2–*n*H3 represents the construct lacking the H3 chain signal output, and H1–H2–H3 represents the construct with both H2 and H3 signal outputs. We then recorded fluorescence spectra for these three groups under identical conditions, both with and without the target. As shown in Fig. 2A and B, a distinct difference in fluorescence signals was observed depending on the presence of miRNA-21, with the target triggering the EDC reaction and facilitating the release of the G4 dimer, which in turn generated the fluorescence signal. Additionally, the fluorescence signal difference observed with H1–H2–H3 was greater than that observed with either H1–*n*H2–H3 or H1–H2–*n*H3, indicating that the dual-output EDC reaction provides higher signal amplification than the single-output EDC reactions. Collectively, the results from AGE and fluorescence spectroscopy demonstrate the feasibility of this biosensing approach.

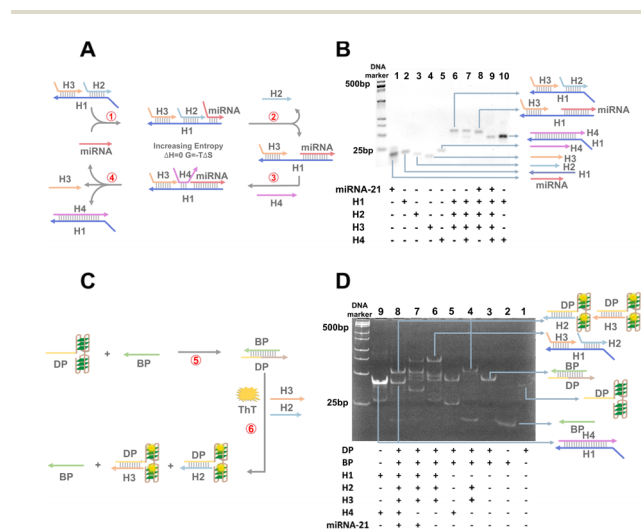


Fig. 1 Schematic diagrams (A and C) and AGE analysis of the (B) EDC dual-signal output amplification process and (D) the entire reaction process. All strands were at a concentration of 1 μM before mixing.

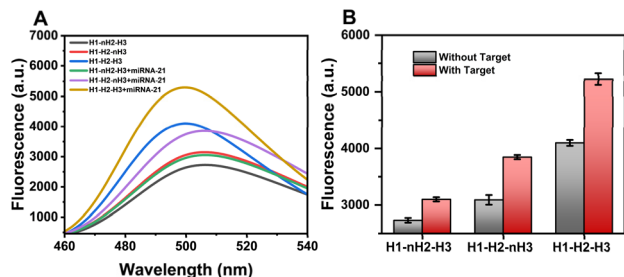


Fig. 2 (A) Fluorescence spectra to validate the binding strategy of the EDC double output reaction with G4 dimers and (B) its graph histogram.

The circular dichroism of DP

In order to verify the successful formation of the G4 dimer and its effective interaction with ThT, we recorded the circular dichroism (CD) spectra of G4 dimer/ThT in the presence of 500 mM Na⁺. As shown in Fig. 3, the CD spectra of the G4 dimer presented strong analytical peaks, with a negative peak at 260 nm and a positive peak at 290 nm, indicative of the dimer adopting an antiparallel topology.⁴⁷ As reported, for the binding mode of G4 dimers with ThT, positive CD bands above 350 nm indicate a groove-binding mode, while negative CD bands above 350 nm indicate an insertion-binding mode.⁴⁵ These observations confirmed the successful formation of the G4 dimer and its effective interaction with ThT.

Performance testing of the constructed strategy

Before conducting performance testing, experimental conditions were optimized to ensure that subsequent experiments were carried out under optimal conditions. The concrete analysis is detailed in Fig. S2. The optimized conditions obtained were as follows: an NaCl concentration of 500 mM, a reaction time of 4 hours, a reaction temperature of 35 °C, and a ratio of H1-H2-H3 to H4 of 1 : 1. Under the aforementioned optimized experimental conditions, the performance of the constructed strategy was analysed. Fig. 4A shows a mechanistic diagram of the fluorescence change of the strategy at different concentrations of miRNA-21. As shown in Fig. 4B, the fluorescence signal of the reaction increased progressively with higher concentrations of miRNA-21, ranging from 0.0001 nM to 0.1 nM. Fig. 4C illustrates a strong correlation between ΔF and the

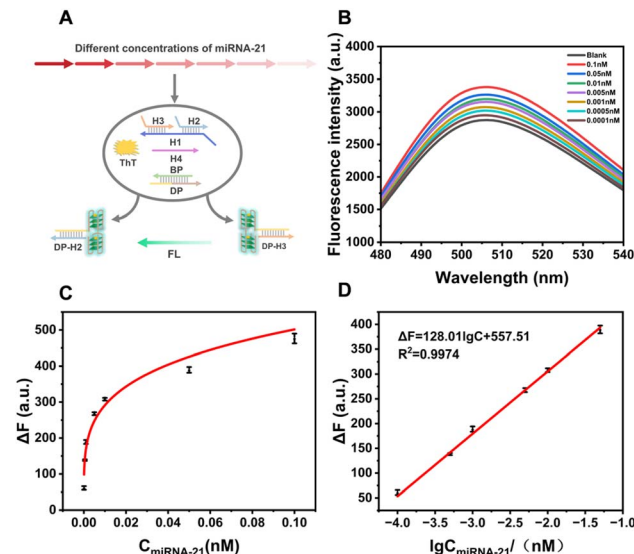


Fig. 4 (A) Illustration depicting the fluorescence produced by different miRNA-21 concentrations in the constructed strategy. (B) Fluorescence emission spectra of this sensor when varying miRNA-21 concentrations are present (0.0001 nM, 0.0005 nM, 0.001 nM, 0.005 nM, 0.01 nM, 0.05 nM, and 0.1 nM). (C) Variation in ΔF in the presence of varying miRNA-21 concentrations. (D) The calibration curve of ΔF versus the logarithms of miRNA-21 concentrations.

concentration change of miRNA-21. As seen in Fig. 4D, the ΔF exhibited a linear relationship with the logarithm of the miRNA-21 concentrations ranging from 0.0001 nM to 0.1 nM, expressed using the linear equation $\Delta F = 128.01 \lg C + 557.51$, with a correlation coefficient (R^2) of 0.9974. The limit of detection was calculated to be 82 fM ($S/N = 3$). In comparison to other methodologies, as summarized in Table 1, our approach demonstrates superior sensitivity for miRNA-21 detection.

Specificity analysis of the constructed strategy

To assess specificity, we also tested two miRNA-21 homologous related miRNAs, including let-7a and let-7b, and mutants M1, M2, and M3. The results in Fig. 5D reveal a marked difference in the intensity of the fluorescent signals generated by miRNA-21 compared to these interferents, indicating that our strategy exhibits excellent specificity for miRNA-21.

Application of biosensors in human serum analysis

To explore the practical applications of the developed biosensor, we conducted standard addition tests with 1% human serum samples. Four concentrations of miRNA-21 (1, 5, 10, and 50 pM) were evaluated, with each concentration assayed in triplicate. The results, shown in Table 2, revealed recoveries ranging from 92.4% to 100%, with relative standard deviations (RSDs) between 1.6% and 2.4%. These findings indicate that the constructed sensor is capable of effectively detecting miRNA-21 in real serum samples.

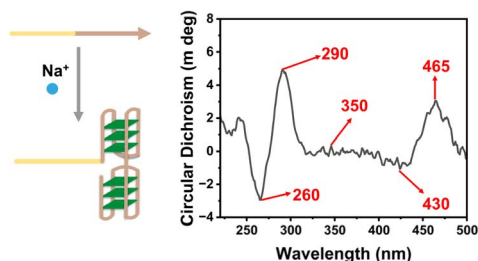
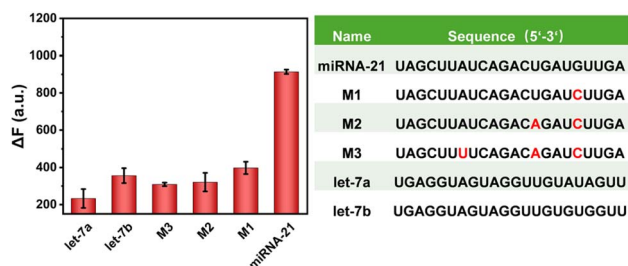


Fig. 3 CD spectrum of DP. Experimental conditions: 5 μ M DP, 20 μ M ThT.

Table 1 Comparison of different enzyme-free methods for miRNA determination

Method	Signal	Linear range	LOD	Ref.
EDC	FL	0.5 to 200 nM	1.86 pM	33
EDC	FL	0.1 to 1 nM	12 pM	48
EDC	FL	0 to 10 nM	10 pM	49
EDC + DNAzyme	FL	0.1 to 100 nM	17 pM	50
EDC + DNAzyme	FL	0.05 to 2 nM	21 pM	32
EDC	FL	0.2 to 2 nM	100 pM	34
DNAAnanosphere + CHA	FL	0.05 to 3.5 nM	2 pM	51
HCR + SDA	FL	100 fM to 50 nM	92.7 fM	52
CHA + HCR	UV	0.010 to 1.0 nM	2.8 pM	53
EDC + G4-dimer	FL	0.1 to 100 pM	82 fM	This work

**Fig. 5** Specificity analysis of the strategy.**Table 2** Recovery experiments for miRNA-21 in 1% real human serum

Sample	Added (pM)	Found (pM)	Recovery (% , <i>n</i> = 3)	RSD (% , <i>n</i> = 3)
1% Serum	1.00	0.92	92.4	2.4
	5.00	5.03	100	1.7
	10.00	9.88	98.8	1.6
	50.00	48.03	96.0	2.0

Conclusions

In conclusion, this study presents a novel fluorescent biosensor aimed at achieving ultrasensitive detection of miRNA-21. By integrating a dual-output EDC amplification system with G4 dimer-mediated fluorescence enhancement, we have introduced several key innovations and advantages: (1) enhanced amplification efficiency. The dual-output configuration surpasses that of conventional single-output EDC systems, maximizing strand utilization and significantly improving amplification efficiency. This advancement enables a remarkable detection limit of 82 fM ($S/N = 3$) within a linear range of 0.1–100 pM ($R^2 = 0.998$); (2) superior fluorescence response. Thanks to the high quantum yield of G4 dimers and their facile activation by EDC output strands, our biosensor achieves substantial fluorescence enhancement, allowing for enhanced signal-to-noise discrimination; (3) label-free and cost-effective platform. The enzyme-free operation eliminates the need for DNA chemical modification or exogenous enzymes, thus

simplifying the process and reducing costs, while maintaining high specificity for discriminating single-/multi-nucleotide mismatches and homologous miRNAs. The modular design of the sensor facilitates its adaptation to detect other miRNA targets by simply reconfiguring the sequence of the EDC output strands. Successful validation in human serum samples yielded recovery rates ranging from 96.2 to 104.8% ($RSD < 5.2\%$), highlighting its clinical potential. This work lays the foundation for a versatile, cost-effective, and scalable platform for nucleic acid detection, offering significant promise for early cancer diagnostics.

Author contributions

Xiaoqing Chen proposed the experimental conceptualization, performed investigation and was responsible for the funding acquisition. Chuan Long mainly conducted a formal analysis and carried out investigation and writing-original draft. Yao Yao mainly completed data curation and writing-original draft. Qi Liu is responsible for the writing-review & editing. Ziyi Gao completed data curation.

Conflicts of interest

There are no conflicts to declare.

Data availability

The data supporting this article have been included as part of the SI.

Materials and reagents, oligonucleotide sequences, Nupack simulation and optimization of experimental conditions. See DOI: <https://doi.org/10.1039/d5ay01060h>.

Acknowledgements

This work was supported by the National Natural Science Fund Regional Innovation and Development Joint Fund Project (No. U22A20617), the National Natural Science Foundation of China (No. 22474157 and 72088101), the Natural Science Foundation of Hunan Province (No. 2024JJ5417), the Innovation-Driven

Project of Central South University (2023CXQD048), the Changsha Natural Science Foundation Project (kq2402199), and the Fundamental Research Funds for the Central Universities of Central South University (2025ZZTS0480).

Notes and references

- H. Sung, J. Ferlay, R. L. Siegel, M. Laversanne, I. Soerjomataram, A. Jemal and F. Bray, *CA. Cancer J. Clin.*, 2021, **71**, 209–249.
- F. Bray, M. Laversanne, H. Sung, J. Ferlay, R. L. Siegel, I. Soerjomataram and A. Jemal, *CA. Cancer J. Clin.*, 2024, **74**, 229–263.
- H. Schwarzenbach, D. S. B. Hoon and K. Pantel, *Nat. Rev. Cancer*, 2011, **11**, 426–437.
- J. Zhao, K. Xia, P. He, G. Wei, X. Zhou and X. Zhang, *Coord. Chem. Rev.*, 2023, **497**, 215456.
- T. Jet, G. Gines, Y. Rondelez and V. Taly, *Chem. Soc. Rev.*, 2021, **50**, 4141–4161.
- T. Kim, *Cancers*, 2020, **12**, 2597.
- J. Tao, Y. Zeng, B. Dai, Y. Liu, X. Pan, L.-Q. Wang, J. Chen, Y. Zhou, Z. Lu, L. Xie and Y. Liang, *Nat. Commun.*, 2023, **14**, 8131.
- A. Kassambara, M. Jourdan, A. Bruyer, N. Robert, V. Pantescio, O. Elemento, B. Klein and J. Moreaux, *Nucleic Acids Res.*, 2017, **45**, 5639–5652.
- H. Gao, E. Nepovimova, Z. Heger, M. Valko, Q. Wu, K. Kuca and V. Adam, *Pharmacol. Res.*, 2023, **194**, 106841.
- S. Zhang, M. Yan, X. Lv, P. Wang, W. Liu, B. Hu, S. Chen and Z. Shao, *Int. J. Nanomed.*, 2025, **20**, 2163–2179.
- L. Ma, S. Ye, X. Wang and J. Zhang, *ACS Sens.*, 2021, **6**, 1392–1399.
- C. Y. Lee, J. Y. Jeong, H. J. Nam and C. A. Hong, *ACS Appl. Mater. Interfaces*, 2025, **17**, 5813–5822.
- C. Chen, *Nucleic Acids Res.*, 2005, **33**, e179.
- S. Jung, W. J. Kim, B. K. Kim, J. Kim, M. J. Kim, K. P. Kim and S. K. Kim, *Biosens. Bioelectron.*, 2020, **163**, 112301.
- X. Wang, H. Chen, M. Sun, B. Chen, H. Xu, Y. Fan, H. Zhou and J. Liu, *Sens. Actuators, B*, 2025, **425**, 137016.
- Y. Zhang, T. Huang, F. Yang, Q. Tan, J. Ye, X. Feng and D. Zhang, *Anal. Chem.*, 2025, **97**(8), 4524–4532.
- D.-M. Yang, D. Li, Q. Zhang, S. Zhao and C.-Y. Zhang, *Anal. Chem.*, 2025, **97**, 3145–3152.
- W. Liu, Y. Yao, Q. Liu and X.-Q. Chen, *Anal. Chem.*, 2024, **96**, 1362–1370.
- M. Cheng, L. Wang, M. Jiang, Y. Bao, M. Fan, H. Shen, X. Zhang, Z. Liu, M. Liu and X. Ran, *Sens. Actuators, B*, 2025, **427**, 137222.
- T. Shen, W. Yuan, Y. Zhang, S. Guo, Y. Xie, Y. Cheng, H. Jia and Y. Wang, *Talanta*, 2025, **286**, 127504.
- Y. Feng, Q. Liu, X. Zhao, M. Chen, X. Sun, H. Li and X. Chen, *Anal. Chem.*, 2022, **94**, 2934–2941.
- W. Liu, Y. Yao, Q. Liu and X. Chen, *Anal. Chem.*, 2024, **96**, 9909–9916.
- Y. Feng, S. Liu, Y. Yao, M. Chen, Q. Liu and X. Chen, *Anal. Chem.*, 2024, **96**, 564–571.
- Y. Yang, D. Kong, Y. Wu, Y. Chen, C. Dai, C. Chen, J. Zhao, S. Luo, W. Liu, Y. Liu and D. Wei, *Anal. Chem.*, 2023, **95**, 13281–13288.
- X. Zhang, W. Chen, S. Wan, B. Qu, F. Liao, D. Cheng, Y. Zhang, Z. Ding, Y. Yang and Q. Yuan, *J. Am. Chem. Soc.*, 2025, **147**, 6679–6687.
- F. Yu, Y. Wang, C.-Y. Wang, G.-Y. Zhu, L.-P. Bai, K. Guo, Z.-H. Jiang and W. Zhang, *Biosens. Bioelectron.*, 2025, **272**, 117093.
- Y. Yao, W. Liu, J. Guan, Y. Cheng, Z. Wu, Q. Liu and X. Chen, *Anal. Chem.*, 2024, **96**, 12012–12021.
- B. Guo, X. Sun, S. Tao, T. Tian and H. Lei, *Anal. Chem.*, 2024, **96**, 19430–19438.
- Y. Zhang, J. Chen, H. Yang, W. Yin, C. Li, Y. Xu, S.-Y. Liu, Z. Dai and X. Zou, *Anal. Chem.*, 2022, **94**, 9665–9673.
- X. Meng, H. Wang, M. Yang, J. Li, F. Yang, K. Zhang, H. Dong and X. Zhang, *Anal. Chem.*, 2021, **93**, 1693–1701.
- X. Zhao, H. Wang, Y. Feng, H. Li, Q. Liu and X. Chen, *Sens. Actuators, B*, 2023, **374**, 132802.
- C. Xing, Q. Lin, X. Gao, T. Cao, J. Chen, J. Liu, Y. Lin, J. Wang and C. Lu, *ACS Appl. Mater. Interfaces*, 2022, **14**, 39866–39872.
- S. Yue, X. Xu, L.-P. Jiang, H. Yao and J.-J. Zhu, *Anal. Chem.*, 2025, **97**, 1739–1747.
- G. Qi, X. Diao, Y. Tian, D. Sun and Y. Jin, *Anal. Chem.*, 2024, **96**, 18519–18527.
- H. Zhou, J. Zhang, B. Li, J. Liu, J.-J. Xu and H.-Y. Chen, *Anal. Chem.*, 2021, **93**, 6120–6127.
- X. Huang, H. Tian, L. Huang, Q. Chen, Y. Yang, R. Zeng, J. Xu, S. Chen, X. Zhou, G. Liu, H. Li, Y. Zhang, J. Zhang, J. Zheng, H. Cai and H. Zhou, *Anal. Chem.*, 2023, **95**, 5955–5966.
- Z. Ye, M. Ma, Y. Chen, R. Liu, Y. Zhang, P. Ma and D. Song, *Anal. Chem.*, 2024, **96**, 3636–3644.
- X. Wen, Y. Chen, Y. He, R. Yuan and S. Chen, *Anal. Chem.*, 2025, **97**, 2094–2102.
- R. Zhang, X. Zhou, H. Deng, R. Yuan and Y. Yuan, *Anal. Chem.*, 2024, **96**, 16735–16742.
- X. He, T. Zeng, Z. Li, G. Wang and N. Ma, *Angew. Chem., Int. Ed.*, 2016, **55**, 3073–3076.
- S. Li, F. Zhang, X. Chen and C. Cai, *Sens. Actuators, B*, 2018, **263**, 87–93.
- P. Zhang, Y. Ouyang, Y. S. Sohn, M. Fadeev, O. Karmi, R. Nechushtai, I. Stein, E. Pikarsky and I. Willner, *ACS Nano*, 2022, **16**, 1791–1801.
- H. Cai, C. Zhou, Q. Yang, T. Ai, Y. Huang, Y. Lv, J. Geng and D. Xiao, *Chin. Chem. Lett.*, 2018, **29**, 531–534.
- Y. Kataoka, H. Fujita, Y. Kasahara, T. Yoshihara, S. Tobita and M. Kuwahara, *Anal. Chem.*, 2014, **86**, 12078–12084.
- J. Mohanty, N. Barooah, V. Dhamodharan, S. Harikrishna, P. I. Pradeepkumar and A. C. Bhasikuttan, *J. Am. Chem. Soc.*, 2013, **135**, 367–376.
- S. Jing, Q. Liu, Y. Jin and B. Li, *Anal. Chem.*, 2021, **93**, 1333–1341.
- A. C. Bhasikuttan and J. Mohanty, *Chem. Commun.*, 2015, **51**, 7581–7597.

- 48 L. Zhang, Q. Zhang, D. Chen, Y. Deng, R. Wang and S. Wang, *Anal. Chem.*, 2024, **96**, 16036–16044.
- 49 L. Li, X. He, Y. Zhang, D. Qi, M. Li, H. Zhang, Q. Shen and Q. Fan, *Anal. Chem.*, 2025, **97**(1), 768–774.
- 50 X. Huang, Z. Li, Y. Shi, Y. Zhang, T. Shen, M. Chen, Z. Huang, Y. Tong, S.-Y. Liu, J. Guo, X. Zou and Z. Dai, *Biosens. Bioelectron.*, 2023, **241**, 115669.
- 51 Y. Wang, L. P. Cao, X. J. Shuai, L. Liu, C. Z. Huang and C. M. Li, *Anal. Chem.*, 2024, **96**, 4597–4604.
- 52 M. Sun, Q. Zhou, J. Peng, S. Liu, J. Luo, L. Bai, W.-J. Duan, J.-X. Chen, Z. Dai and J. Chen, *Anal. Chem.*, 2024, **96**(22), 9078–9087.
- 53 Z. Wang, Y. Shang, Y. Zhu, Y. He, Y. Chen, X. Liu and F. Wang, *Anal. Chem.*, 2024, **96**, 5560–5569.